Multimodal analysis reveals genes driving neuronal maturation in the primate prefrontal cortex

Yu Gao[1,+], Qiping Dong[1,+], Kalpana Hanthanan Arachchilage[1,+], Ryan D. Risgaard[1], Jie Sheng[1], Moosa Syed[1], Danielle K. Schmidt[1], Ting Jin[1], Shuang Liu[1], Sara Knaack[1], Dan Doherty[2], Ian Glass[2], Jon E. Levine[3,4], Daifeng Wang[1,5,6*], Qiang Chang[1,7,8*], Xinyu Zhao[1,3*], André M. M. Sousa[1,3*]

[1]Waisman Center, University of Wisconsin-Madison; Madison, WI, USA

[2]Department of Pediatrics, University of Washington School of Medicine; Seattle, WA, USA

[3]Department of Neuroscience, University of Wisconsin-Madison; Madison, WI, USA

[4]Wisconsin National Primate Research Center, University of Wisconsin-Madison; Madison, WI 53705

[5]Department of Biostatistics and Medical Informatics, University of Wisconsin-Madison; Madison, WI, USA

[6]Department of Computer Sciences, University of Wisconsin-Madison; Madison, WI, USA

[7]Department of Medical Genetics, University of Wisconsin-Madison; Madison, WI, USA

[8]Department of Neurology, University of Wisconsin-Madison; Madison, WI, USA

+These authors contributed equally to this work.

*Correspondence to Andre M. M. Sousa (andre.sousa@wisc.edu), Xinyu Zhao (xinyu.zhao@wisc.edu), Qiang Chang (qchang@waisman.wisc.edu), Daifeng Wang (daifeng.wang@wisc.edu)

Abstract

The dorsolateral prefrontal cortex (dlPFC) is an evolutionarily derived cortical region in primates critical for high-level cognitive functions and implicated in various neuropsychiatric disorders[1-8]. The cells that compose the dlPFC, especially excitatory and inhibitory neurons, undergo extensive maturation throughout midfetal and late-fetal development, during which critical neurodevelopmental events, such as circuit assembly and electrophysiological maturation of neurons, occur[3,8-15]. Despite the relevance of neuronal maturation in several neurodevelopmental and psychiatric disorders[8,16], the molecular mechanisms underlying this process remain largely unknown. Here, we performed an integrated Patch-seq and single-nucleus multiomic analysis of the rhesus macaque dlPFC to identify genes governing neuronal maturation from midfetal to late-fetal development. Our multimodal analysis identified gene pathways and regulatory networks important for the maturation of distinct neuronal populations, including upper-layer intratelencephalic-projecting neurons. We identified genes underlying the maturation of specific electrophysiological properties of these neurons. Furthermore, gene knockdown in organotypic slices revealed that *RAPGEF4* regulates the maturation of resting membrane potential and inward sodium current. Using this strategy, we also found that the knockdown of *CHD8*, a high-confidence autism spectrum disorder risk gene, in human slices led to deficits in neuronal maturation, via the downstream downregulation of several key genes, including *RAPGEF4*. Our study revealed novel regulators of neuronal maturation during a critical period of prefrontal development in primates and implicated such regulators in molecular processes underlying autism.

Introduction

During neocortical development, after postmitotic excitatory neurons acquire their specific laminar and projection identities, they undergo dynamic morphological and functional maturation. Although we have a robust knowledge of the molecular and cellular mechanisms that govern cell fate specification during cortical development[9-15], and of the transcriptomic and electrophysiological properties of mature neurons in the adult neocortex[17-21], our understanding of the gene networks that regulate the early stages of electrophysiological maturation of neurons remains elusive. The dorsolateral prefrontal cortex (dlPFC), a neocortical area highly derived in primates[1-3], is involved in myriad higher-order brain functions, including executive functions such as working memory, planning, and decision-making[3-5]. These functions are significantly impaired in brain disorders, including autism spectrum disorders (ASD), schizophrenia, and obsessive-compulsive disorder[6-8]. The neurons in the primate dlPFC undergo extensive maturation during midfetal and late-fetal development, a convergent period of expression for many ASD genes[22,23]. Therefore, a multimodal profiling of primate dlPFC neurons that combines electrophysiological and genomic analyses during critical periods for neuronal maturation is essential to understand the mechanisms driving neuronal maturation.

Study design

To uncover the molecular mechanisms that regulate the maturation of dlPFC neurons, we performed single-nucleus multiomic (snMultiomic) analyses of the dlPFC from 9 rhesus macaques (*Macaca mulatta)*, ranging from postconceptional day (PCD) 85 to PCD155 (**Fig. 1**). In addition, to infer how gene expression regulated the electrophysiological maturation of neurons, we performed Patch-seq on acute dlPFC slices from 16 macaques, including the same specimens

profiled for snMultiome. This approach allowed us to integrate our electrophysiological analyses with gene expression profiles and to identify the genes that are important for the maturation of specific electrophysiological features. Furthermore, we have evaluated the function of selected genes – *RAPGEF4* and *CHD8* – and demonstrated that a loss of function of these genes affects the morphological and electrophysiological maturation of cortical neurons in organotypic slices of macaque and human.

Transcriptomic changes underlying the maturation of rhesus macaque dlPFC cells during midfetal and late-fetal development

We performed snMultiomic analyses on 9 rhesus macaque dlPFC samples across eight prenatal ages: PCD85, PCD95, PCD100, PCD105, PCD110, PCD125, PCD145, and two PCD155 (**Fig. 2a, Supplementary Table 1**). After implementing stringent quality control measures, we retained 76,855 nuclei for further analyses (**Extended Data Fig. 1, Supplementary Tables 1-2**). After removing batch effects, we used unsupervised clustering to group nuclei into transcriptomically defined groups (**Extended Data Fig. 1b-c**). Using this strategy, together with cell type-specific marker genes[9,17,24], we defined 9 major cell classes that included glutamatergic excitatory neurons (ExN), GABAergic inhibitory neurons (InN), glial progenitor cells (GPC), astrocytes, oligodendrocyte precursor cells (OPC), oligodendrocytes, microglia, vascular leptomeningeal cells (VLMC), and endothelial cells (**Extended Data Fig. 2a**). We re-clustered the ExN and InN nuclei to identify their subclasses based on the layer (L) and projection identity (intratelencephalic [IT], extratelencephalic [ET], near-projecting [NP], corticothalamic [CT], and L6B) for ExN, and the developmental origin (medial ganglionic eminence [MGE], caudal ganglionic eminence [CGE], or dorsal lateral ganglionic eminence [dLGE]) for InN (**Fig. 2b; Extended Data Fig. 2b-**

c). Interestingly, one small population of IT neurons exhibited molecular features of both ExN L2-3 IT and ExN L3-5 IT, indicating that this small population of neurons is yet to be fully specified; we classified this population as ExN L2-3 IT/L3-5 IT. At the lowest hierarchical level of cell type classification, we transcriptomically defined 85 cell subtypes (**Supplementary Table 3; Extended Data Fig. 2e**). By integrating our dataset with two published snRNA-seq datasets that analyzed early fetal[24] and adult[17] macaque dlPFC, we observed that our data bridges the embryonic/early fetal cell types with the adult cell types, facilitating the tracing of the developmental origins of distinct adult cell subtypes (**Extended Data Fig. 3**).

As expected, we observed an increasing number of glial cells, including astrocytes, OPCs, and oligodendrocytes throughout late-fetal development (**Fig. 2c**), a period characterized by minimal cortical neurogenesis and robust gliogenesis[25]. Within the excitatory neurons, we observed that the intratelencephalic-projecting (IT) neurons were more abundant than any other subclass, as previously described in the adult dlPFC[17]. The selective expansion of IT neurons in the primate lineage, especially of upper-layer (L2-3) neurons[17] and their functional relevance in the cortico-cortical circuits that govern some of the unique cognitive and behavioral abilities of primates[26], led us to focus our analysis on the maturational profiles of these IT neuronal populations: ExN L2-3 IT and ExN L3-5 IT (**Fig. 2d-g**). We performed differential gene expression analysis along the developmental trajectory (i.e., pseudotime) to identify genes that display dynamic, highly variable changes during neuronal maturation. Among the top 100 genes (**Supplementary Table 4**), we observed genes that exhibit cell type-specific correlation with maturation (**Fig. 2e, g**), including *MEIS2*, a transcriptional regulator that is induced by retinoic acid and is important for the arealization of the prefrontal cortex[27], in L2-3 IT, and *FOXP2*, a gene encoding a transcription factor that has recently been shown to have primate-specific expression

in L3-5 IT excitatory neurons[17]. Disruptions in these genes have been linked to neuropsychiatric disorders[16,28].

Together, our analyses uncovered the transcriptional landscape of primate midfetal and late-fetal prefrontal cortical development, highlighting differences between distinct excitatory neuronal populations throughout maturation.

Chromatin accessibility signatures and gene regulatory networks of macaque midfetal and late-fetal dlPFC cells

The simultaneous profiling of gene expression and chromatin accessibility allows linking putative regulatory elements to genes, thus providing insights into cell-type gene regulatory mechanisms in the developing primate brain. After filtering out low-quality nuclei and implementing other stringent quality control steps, snATAC-seq data from 64,941 nuclei were retained for downstream analyses (**Extended Data Fig. 1d-h**). We observed that the clustering of cells based on accessible chromatin was similar to the clustering utilizing gene expression data (**Extended Data Fig. 1g-h**), showing the congruence between the two datasets (**Fig. 3a**). However, the snATAC-seq data revealed more pronounced differences in the maturation states of cells within each cell subclass, especially for IT excitatory neurons (**Extended Data Fig. 1e**). To gain a better understanding of the association of regulatory elements and their target genes during neuronal maturation, we estimated peak-to-gene links, which identify co-activity between genes and their nearby accessible chromatin regions, for the excitatory and inhibitory neurons (**Extended Data Fig. 4a**), thus providing a list of potential regulatory elements for each gene (**Supplementary Table 5**). We found that peak-gene combinations were hierarchically divided into three distinct categories: a cluster specific to excitatory neurons during early midfetal development, a cluster

specific to excitatory neurons during late-fetal development, and a cluster specific to inhibitory neurons during late-fetal development. Functional enrichment analysis of each group revealed that the clusters specific to late-fetal development were enriched for terms related to calcium signaling and dendritic development in excitatory neurons, and synaptic processes in inhibitory neurons, whereas the early-midfetal development cluster was enriched for transcriptional regulation terms (**Extended data Fig. 4b-d**).

Next, since gene expression is regulated by gene regulatory networks (GRNs) [29] and expression of genes associated with ASD converge in excitatory neurons during these developmental stages in ExN L2-3 IT and ExN L3-5 IT cell subclasses[22,23], we inferred cell-type gene regulatory networks (GRNs) for these two cell subclasses using transcriptomic and epigenomic data together with transcription factor (TF) motif binding sites (**Methods**). These cell-type GRNs link regulatory elements with TF binding sites to target genes. We particularly focused on analyzing the subnetworks regulating the genes identified in our developmental maturation trajectory analysis (**Supplementary Table 4**) and found nine major TFs regulating the driver genes of the two cell subclasses. Among these nine TFs, we identified FOXP2 as a hub TF for ExN L3-5 IT, MEIS2 as a key regulator for ExN L2-3 IT, and MEF2C as an important TF for both ExN subclasses (**Fig. 3b**).

To identify putative regulatory elements that underlie the transcriptomic differences between ExN L2-3 IT and ExN L3-5 IT, we calculated differential accessibility and overrepresented motifs between these neuronal populations throughout midfetal and late-fetal development. Using this strategy, we identified the MEIS2 motif MA0774.1 as one of the overrepresented motifs in the ExN L2-3 IT subclass (**Supplementary Table 6**). Furthermore, we found that ExN L2-3 IT has both higher *MEIS2* gene expression and a higher MEIS2 motif activity

score when compared to ExN L3-5 IT (**Fig. 3c**). Because MEIS2 is a transcription factor enriched in upper-layer neurons in primates[17,27] and is implicated in neuropsychiatric disorders[28], we calculated MEIS2 transcription factor footprints across the whole genome in the two cell subclasses and found that, throughout the analyzed developmental periods, ExN L2-3 IT had a higher footprint enrichment than ExN L3-5 IT, with the highest enrichment in ExN L2-3 IT during midfetal development (PCD105-110) and the lowest footprint enrichment in ExN L3-5 IT during late fetal development (PCD155), indicating the selective involvement of MEIS2 in the regulation of target genes in ExN L2-3 IT (**Fig. 3c**). Indeed, quantitative immunofluorescence showed that there were significantly fewer MEIS2-expressing cells in L3-5, identified by the expression of *RORB* (**Extended Data Fig. 4e**), compared to L2-3 of dlPFC at PCD155 (**Fig. 3d**).

One of the genes potentially regulated by MEIS2 in IT excitatory neurons is the *Nuclear factor I/A* (*NFIA*), a gene known to be regulated by MEIS2 in retinal progenitor cells[30] which has been linked to callosal hypoplasia, likely reflecting malformations of upper-layer excitatory neurons[31]. By analyzing the distribution of accessible chromatin peaks in the vicinity of *NFIA* across the two neuronal subclasses and developmental periods, we identified 5 active MEIS2 binding sites within 200kb upstream of the *NFIA* transcription start site (**Fig. 3e**). We also found three peak-to-gene links (peaks that show higher co-activity with *NFIA* gene expression), with one of the links containing two predicted MEIS2 binding motifs (chr1-163553896-163555161) approximately 181kb upstream of the *NFIA* transcription starting site, suggesting that it may be a potential regulatory element for *NFIA*. To validate this finding, we conducted a dual luciferase assay to assess the activity of the genomic sequence containing the two MEIS2 motifs. Overexpression of MEIS2 resulted in a significant increase in transcription activity driven by the

genomic sequence. Furthermore, when we introduced mutations into two potential MEIS2 binding motifs, one of these mutations significantly reduced the activity of the genomic sequence (**Fig. 3f**).

Patch-seq of midfetal and late-fetal macaque dlPFC cells identified transcriptomic signatures defining electrophysiological maturation

The midfetal and late-fetal periods are critical stages in cortical development, marked by notable alterations in neuronal morphology, electrophysiology, and gene expression[32]. Although all the analyzed neurons displayed a relatively immature morphology, PCD155 neurons exhibited significantly greater complexity, with greater total dendritic length, increased branching points, and more endings when compared to neurons from PCD100 brains (**Extended Data Fig. 5**). To gain a comprehensive understanding of the molecular mechanisms that drive neuronal maturation, we employed Patch-seq, which allows for electrophysiological and transcriptomic analyses of the same cell[33], in 16 rhesus macaques ranging from PCD85 to PCD155 (**Fig. 4a, Extended Data Fig. 5g-h, Supplementary Tables 1**). We used our snRNA-seq data (**Fig. 2**) as the reference dataset to infer cell types by mapping the 256 cells profiled by Patch-seq onto the reference UMAP (**Fig. 4b, Supplementary Table 7, Extended Data Fig. 5i**). Approximately 72% of all cells were identified as neurons, which included 111 IT neurons (**Supplementary Table 7**). In order to evaluate the similarity among the IT neurons, we investigated the electrophysiological features of three major IT subtypes (L2-3, L3-5, and L6) across different ages. Our findings revealed that these IT neurons exhibited comparable electrophysiological features (**Extended Data Fig.6a-e**). Therefore, we combined all IT neuron types for downstream analysis.

We employed a pseudotime trajectory analysis to infer a maturation trajectory by integrating differentially expressed genes across age groups in all identified IT neurons (**Methods**).

Our analysis revealed a trajectory characterized by the progressive maturation of IT neurons from earlier to later developmental periods (**Fig. 4c**). We observed that the proportion of IT neurons exhibiting action potentials (APs) across six age groups (PCD85-90, PCD95-100, PCD105-110, PCD125, PCD145, and PCD155) gradually increased from 0% in the PCD85-90 group to 95% in PCD155, providing strong evidence for electrophysiological maturation (**Extended Data Fig. 6f**). We then assessed neuronal maturation through the lens of the following features that offer unique perspectives on maturation: membrane capacitance (C_m), input resistance (R_{in}), resting membrane potential (RMP), and inward sodium current (I_{Na}). Our analysis revealed that, during early midfetal development (from PCD85 to PCD100), none of the electrophysiological features showed significant change (**Fig. 4e-h**). We observed a significant increase in C_m from PCD100 to PCD105, after which the values remained stable (**Fig. 4e**). This increase in C_m potentially reflects the enlargement of the cell body and more complex cellular structures during the maturation of neurons. In contrast, there was a gradual decline in the averaged value of R_{in} after PCD100 (**Fig. 4f**). This effect may be attributed to an increase in the number of ion channels in the neuronal membrane. Moreover, the morphological changes that occur in dendrites (**Extended Data Fig. 5b-f**) and spines during maturation may contribute to alterations in signal processing and integration, further enhancing neuronal function. We also observed a conspicuous pattern of increasingly negative RMP from PCD100 to PCD155 (**Fig. 4g**), which reflects the developmental maturation in the ion channel composition of these neurons, allowing for improved electrical signal processing and transmission. During neuronal development, the current density of I_{Na} amplifies, thereby increasing the capacity of neurons to generate action potentials. Our results indicate a significant increase in the magnitude of the I_{Na} from PCD105 to PCD155 (**Fig. 4h**). This suggests that IT neurons in the dlPFC acquire the ability to initiate and transmit APs after PCD105. In summary,

our analyses showed a progression in maturation across four distinct electrophysiological properties. However, it is noteworthy that the temporal dynamics of the four electrophysiological properties were not identical. While RMP and I_{Na} exhibited a progressive decrease from PCD95-100 to PCD155, C_m and R_{in} displayed drastic changes only at PCD105-110. Our study has uncovered distinct profiles in the temporal dynamics of electrophysiological maturation, where each property exhibits a different rate of maturation.

Similar to IT ExNs, InNs exhibited progressively more negative RMP and I_{Na} from PCD105-110 to PCD155, whereas R_{in} didn't show any significant differences and C_m became higher throughout development (**Extended Data Fig.7a-d**). The proportion of InNs with APs increased from 12.5% in PCD85-90 to 100% in PCD125, PCD145, and PCD155, indicating a faster electrophysiological maturation than ExNs (**Extended Data Fig.7f**).

We hypothesized that differential expression of distinct genes drives the divergent trends of the four electrophysiological features across maturation. By implementing a correlation analysis between the electrophysiological data and the gene expression levels across all IT neurons, we identified 135, 163, 193, and 142 genes that are associated with the electrophysiological features of C_m, R_{in}, RMP, and I_{Na}, respectively (**Extended Data Fig. 8a, Supplementary Table 9**). Importantly, genes that are not expected to exhibit correlation with electrophysiological features, including the housekeeping genes *GAPDH* and *TBP*, showed no significant correlation with any of the electrophysiological features (**Extended Data Fig.8b**). Several genes, including *CAMK2A* and *MICAL2*, exhibited high correlation with all four investigated electrophysiological features (**Fig. 4i-l**). Other genes, such as *RAPGEF4*, exhibited significant correlation with one or two of the electrophysiological features. To validate our Patch-seq data, we performed in situ hybridization on dlPFC sections of PCD100 and PCD155 macaques for select genes that

demonstrated significant correlation with all (*CAMK2A*, *MICAL2*) or some (*RAPGEF4*, *NRGN*) of the electrophysiological features. Consistent with the Patch-seq results, the expression levels of all tested genes were significantly higher in PCD155 compared to PCD100 (**Fig. 4d, Extended Data Fig. 8c**).

Therefore, our Patch-seq analysis of dlPFC neurons across midfetal and late-fetal development revealed evidence of neuronal maturation across three distinct aspects: morphological, transcriptomic, and electrophysiological properties, and identified genes associated with maturation of specific electrophysiological features.

RAPGEF4 **is crucial for the morphological and electrophysiological maturation of excitatory neurons**

Our Patch-seq analysis demonstrated a marked upregulation of *RAPGEF4* expression in IT neurons during cortical development (**Fig. 4k-l**), which was also corroborated by our snRNA-seq data (**Fig. 5a**). RAPGEF4 (Rap Guanine Nucleotide Exchange Factor 4), also known as EPAC2 (exchange protein directly activated by cyclic AMP 2), is a regulator of small GTPase signaling and a protein kinase A (PKA)-independent cAMP target[34,35]. We found that *RAPGEF4* expression exhibited a high degree of correlation with various electrophysiological features, with the highest correlation observed with I_{Na} (r = -0.57) and the second highest correlation with RMP (r = -0.47) (**Extended Data Fig. 9a**). To confirm that RAPGEF4 is required for neuronal maturation, we infected ex vivo macaque brain slices with lentivirus (LV) expressing mScarlet and shRNA against *RAPGEF4* (LV-sh*RAPGEF4*) together with LV expressing mNeonGreen and control shRNA (LV-sh*NC*) (**Fig. 5b**). The neurons with *RAPGEF4* knockdown (sh*RAPGEF4*, mScarlet+) exhibited

reduced dendritic complexity, total dendritic length, branching points, and number of endings compared to controls (mNeonGreen+mScarlet-) (**Fig. 5c-h**). In addition, LV-sh*RAPGEF4*-infected neurons exhibited smaller I_{Na} (**Fig. 5i, j**) and less negative RMP (**Fig. 5i, k**), without significant changes in C_m and R_{in}, compared to control neurons (**Fig. 5l-m, Supplementary Table 10**). These results indicate that a deficiency of *RAPGEF4* in neurons leads to abnormal maturation of I_{Na} and RMP, which is consistent with our finding that *RAPGEF4* had a strong correlation with I_{Na} and RMP (**Fig. 4k-l, Extended Data Fig.9a**).

RAPGEF4 is enriched in neurons compared to other cell types[36]. The levels of *RAPGEF4* increase in the human cortex throughout development, compared to other brain regions or organs (**Extended Data Fig. 9d**) [37,38]. Based on our observations in macaque, we hypothesized that *RAPGEF4* expression is also associated with the maturation of electrophysiological properties in human. We infected human midfetal cortical brain slices with LV-sh*RAPGEF4* and performed patch-clamp recording. As in macaque, we observed reduced I_{Na} and RMP, but not C_m and R_{in}, in LV-sh*RAPGEF4*-infected compared to LV-sh*NC*-infected neurons (**Extended Data Fig.9 e-j, Supplementary Table 10**). To confirm that the observed effect was not caused by off-target effects of the shRNA, we replicated the experiment and observed the same results using a different shRNA targeting *RAPGEF4* in human neurons (**Extended Data Fig. 9k-p**). The role of RAPGEF4 in regulating RMP and I_{Na} maturation in both macaque and human neurons is consistent with the functional enrichment for "regulation of GTPase activity" in genes driving neuronal maturation (**Extended Data Fig. 8d**). These data validate our approach to identify genes that drive the maturation of specific electrophysiological features and reveal the novel role of *RAPGEF4* in morphological and electrophysiological maturation of neurons in both macaque and human cortical development.

***CHD8* knockdown leads to impaired maturation of human cortical excitatory neurons**

Recent advances in genomics have revealed important roles of chromatin regulators during midfetal PFC development and their implications in neurodevelopmental disorders[39,40]. CHD8 (Chromodomain Helicase DNA-binding protein 8) is a chromatin remodeling protein that plays a crucial role in gene expression regulation during brain development and has been linked to ASD[40-44]. To investigate the role of *CHD8* during human midfetal dlPFC development, a critical developmental period for ASD[22,23], we knocked down *CHD8* expression in ex vivo human midfetal brain slices using LV expressing sh*CHD8* and mScarlet together with LV expressing *shNC* and mNeonGreen (**Fig. 6a, Extended Data Fig.10b-c**). LV-sh*CHD8*-infected neurons displayed significantly shorter dendrites compared to control neurons (**Fig. 6b, d-e, Extended Data Fig.10d-f**), suggesting that a deficiency in *CHD8* disrupts morphological maturation of cortical neurons during midfetal development, which is consistent with previous findings in mice[42].

We then performed Patch-seq on 156 cells from slices that contained both *CHD8*-knockdown and control cells (**Fig. 6a, Extended Data Fig. 10g**). To determine the cellular identity of recorded cells, we compared their transcriptome with the reference snRNA-seq data and assigned each queried cell a specific cell type (**Fig. 6c, Extended Data Fig. 10h**, **Supplementary Table 11**). Out of the 156 cells examined, there were 55 excitatory neurons infected with LV-sh*NC* and 42 infected with LV-sh*CHD8* (**Supplementary Table 11**). LV-sh*CHD8*-infected excitatory neurons had a significant increase in both R_{in} and RMP (**Fig. 6i, j**) but not in C_m and I_{Na} (**Fig. 6h, k, Extended Data Fig.10i**), compared to the controls. To rule out the possibility that the observed effect is due to shRNA off-target effects, we repeated the experiment with an alternative

shRNA in human cultured neurons and observed similar deficits in both R_{in} and RMP (**Extended Data Fig. 10j-o**). To determine which genes might underlie the observed differences in R_{in} and RMP maturation caused by *CHD8* knockdown, we identified the differentially expressed genes between LV-sh*CHD8* and LV-sh*NC* and intersected this list with the genes that were associated with the maturation of each electrophysiological feature (**Supplementary Table 9**). We found 10 genes associated with R_{in}, 11 genes associated with RMP, and 20 genes associated with both (**Fig. 6l-p**). These included genes that are associated with the overall maturation of neurons, such as *NRGN* and *CACNA1I*, the R_{in}-associated *RGS6*, a GTPase regulator important for activity-dependent morphological and electrical maturation[45], and *RAPGEF4*, which we showed to significantly impact the maturation of neurons, including proper maturation of RMP (**Fig. 5**). Therefore, *CHD8* knockdown produces a discernible impact on the electrophysiological properties of midfetal human neurons, which is consistent with its role during early development[42,43].

Conclusions

In this study, we employed multimodal approaches including snMultiome and Patch-seq to interrogate mechanisms driving neuronal maturation in the primate dlPFC during midfetal and late-fetal development. We identified differences across cell types in their maturation trajectories as well as critical developmental periods for the maturation of specific electrophysiological properties in excitatory and inhibitory neurons.

We confirmed that, based on their molecular profiles, excitatory neurons gain their laminar and projection identities earlier than interneuronal final specification. This corroborates previous findings that pointed to the relevance of extrinsic factors to the final specification of interneurons

during perinatal development[13,46]. We focused our analyses on the IT excitatory neurons due to their relevance both to primate brain evolution and their association to neuropsychiatric disorders. Our integrative analysis of gene regulatory networks highlighted MEIS2 as a key transcriptional factor for L2-3 IT neuronal development and maturation.

By integrating electrophysiology, morphology, and functional genomics analyses of primate dlPFC development, we were able to discover that different electrophysiological properties mature at different rates. We have uncovered genes that are associated with maturation of specific electrophysiological features that likely underlie the differences we observed in maturation. This led us to functionally evaluate the role of *RAPGEF4*, which was identified as being relevant for the maturation of resting membrane potentials and inward sodium currents. RAPGEF4, a direct target of cAMP, has been shown to regulate dendritic spine remodeling in mice and its deficiency in mice leads to learning and memory deficits[36,47]. However, its role in primate brain development or human disease is unknown. Dysregulation of the cAMP pathway has been implicated in a wide range of neurological disorders and a potential treatment to elevate cAMP levels is currently in clinical trial for fragile X syndrome[48,49]. Our study demonstrates that RAPGEF4 may be one of the small GTPase regulators driving neuronal maturation during primate brain development, especially for RMP, an electrophysiological feature regulated by GTPase signaling.

Finally, to demonstrate the potential of our experimental platform in exploring the developmental origin of human diseases, we showed that knocking down of a high-confidence ASD gene – *CHD8* – impaired morphological and electrophysiological maturation of excitatory neurons in human and macaque organotypic slices. This impairment was driven by the downregulation of the expression of several key genes, including *RAPGEF4 and RGS6*, two

regulators of small GTPase signaling critical for neuronal maturation[50]. This finding shed light on how a chromatin remodeler may regulate the physiological maturation of neurons, thus impairing their normal functioning.

Together, our study has revealed key genes and gene networks driving neuronal maturation during a critical period of prefrontal development in primates and linked the function of a novel regulator of the maturation of specific electrophysiological features with a high-confidence ASD risk gene. Our results demonstrate the power of our multimodal approach and its application for future studies aiming at understanding how genes regulate neuronal maturation and its implication in brain disorders.

References

1 Preuss, T. M. & Wise, S. P. Evolution of prefrontal cortex. *Neuropsychopharmacology* **47**, 3-19 (2022). https://doi.org/10.1038/s41386-021-01076-5

2 Smaers, J. B., Gomez-Robles, A., Parks, A. N. & Sherwood, C. C. Exceptional Evolutionary Expansion of Prefrontal Cortex in Great Apes and Humans. *Curr Biol* **27**, 1549 (2017). https://doi.org/10.1016/j.cub.2017.05.015

3 Sousa, A. M. M., Meyer, K. A., Santpere, G., Gulden, F. O. & Sestan, N. Evolution of the Human Nervous System Function, Structure, and Development. *Cell* **170**, 226-247 (2017). https://doi.org/10.1016/j.cell.2017.06.036

4 Levy, R. & Goldman-Rakic, P. S. Association of storage and processing functions in the dorsolateral prefrontal cortex of the nonhuman primate. *J Neurosci* **19**, 5149-5158 (1999). https://doi.org/10.1523/JNEUROSCI.19-12-05149.1999

5 Kritzer, M. F. & Goldman-Rakic, P. S. Intrinsic circuit organization of the major layers and sublayers of the dorsolateral prefrontal cortex in the rhesus monkey. *J Comp Neurol* **359**, 131-143 (1995). https://doi.org/10.1002/cne.903590109

6 Lewis, D. A. & Mirnics, K. Transcriptome alterations in schizophrenia: disturbing the functional architecture of the dorsolateral prefrontal cortex. *Prog Brain Res* **158**, 141-152 (2006). https://doi.org/10.1016/S0079-6123(06)58007-0

7 Cools, R. & Arnsten, A. F. T. Neuromodulation of prefrontal cortex cognitive function in primates: the powerful roles of monoamines and acetylcholine. *Neuropsychopharmacology* **47**, 309-328 (2022). https://doi.org/10.1038/s41386-021-01100-8

8 Pattabiraman, K., Muchnik, S. K. & Sestan, N. The evolution of the human brain and disease susceptibility. *Curr Opin Genet Dev* **65**, 91-97 (2020). https://doi.org/10.1016/j.gde.2020.05.004
9 Schmitz, M. T. *et al.* The development and evolution of inhibitory neurons in primate cerebrum. *Nature* **603**, 871-877 (2022). https://doi.org/10.1038/s41586-022-04510-w
10 Nowakowski, T. J. *et al.* Spatiotemporal gene expression trajectories reveal developmental hierarchies of the human cortex. *Science* **358**, 1318-1323 (2017). https://doi.org/10.1126/science.aap8809
11 Bhaduri, A. *et al.* An atlas of cortical arealization identifies dynamic molecular signatures. *Nature* **598**, 200-204 (2021). https://doi.org/10.1038/s41586-021-03910-8
12 Johnson, M. B. & Walsh, C. A. Cerebral cortical neuron diversity and development at single-cell resolution. *Curr Opin Neurobiol* **42**, 9-16 (2017). https://doi.org/10.1016/j.conb.2016.11.001
13 Lim, L., Mi, D., Llorca, A. & Marin, O. Development and Functional Diversification of Cortical Interneurons. *Neuron* **100**, 294-313 (2018). https://doi.org/10.1016/j.neuron.2018.10.009
14 Bandler, R. C., Mayer, C. & Fishell, G. Cortical interneuron specification: the juncture of genes, time and geometry. *Curr Opin Neurobiol* **42**, 17-24 (2017). https://doi.org/10.1016/j.conb.2016.10.003
15 Molyneaux, B. J., Arlotta, P., Menezes, J. R. L. & Macklis, J. D. Neuronal subtype specification in the cerebral cortex. *Nat Rev Neurosci* **8**, 427-437 (2007). https://doi.org/Doi 10.1038/Nrn2151
16 Li, M. *et al.* Integrative functional genomic analysis of human brain development and neuropsychiatric risks. *Science* **362** (2018). https://doi.org/10.1126/science.aat7615
17 Ma, S. *et al.* Molecular and cellular evolution of the primate dorsolateral prefrontal cortex. *Science* **377**, eabo7257 (2022). https://doi.org/10.1126/science.abo7257
18 Berg, J. *et al.* Human neocortical expansion involves glutamatergic neuron diversification. *Nature* **598**, 151-158 (2021). https://doi.org/10.1038/s41586-021-03813-8
19 Krienen, F. M. *et al.* Innovations present in the primate interneuron repertoire. *Nature* **586**, 262-269 (2020). https://doi.org/10.1038/s41586-020-2781-z
20 Beaulieu-Laroche, L. *et al.* Allometric rules for mammalian cortical layer 5 neuron biophysics. *Nature* **600**, 274-278 (2021). https://doi.org/10.1038/s41586-021-04072-3
21 Caglayan, E. *et al.* Molecular features driving cellular complexity of human brain evolution. *Nature* **620**, 145-153 (2023). https://doi.org/10.1038/s41586-023-06338-4
22 Willsey, A. J. *et al.* Coexpression networks implicate human midfetal deep cortical projection neurons in the pathogenesis of autism. *Cell* **155**, 997-1007 (2013). https://doi.org/10.1016/j.cell.2013.10.020
23 Parikshak, N. N. *et al.* Integrative functional genomic analyses implicate specific molecular pathways and circuits in autism. *Cell* **155**, 1008-1021 (2013). https://doi.org/10.1016/j.cell.2013.10.031
24 Micali, N. *et al.* Molecular programs of regional specification and neural stem cell fate progression in macaque telencephalon. *Science* **382**, eadf3786 (2023). https://doi.org/10.1126/science.adf3786
25 Rash, B. G. *et al.* Gliogenesis in the outer subventricular zone promotes enlargement and gyrification of the primate cerebrum. *Proceedings of the National Academy of Sciences of*

the United States of America **116**, 7089-7094 (2019). https://doi.org/10.1073/pnas.1822169116

26 Luria, V., Ma, S., Shibata, M., Pattabiraman, K. & Sestan, N. Molecular and cellular mechanisms of human cortical connectivity. *Curr Opin Neurobiol* **80**, 102699 (2023). https://doi.org/10.1016/j.conb.2023.102699

27 Shibata, M. *et al.* Regulation of prefrontal patterning and connectivity by retinoic acid. *Nature* **598**, 483-488 (2021). https://doi.org/10.1038/s41586-021-03953-x

28 Erdogan, F. *et al.* Characterization of a 5.3 Mb deletion in 15q14 by comparative genomic hybridization using a whole genome "tiling path" BAC array in a girl with heart defect, cleft palate, and developmental delay. *Am J Med Genet A* **143A**, 172-178 (2007). https://doi.org/10.1002/ajmg.a.31541

29 Jin, T. *et al.* scGRNom: a computational pipeline of integrative multi-omics analyses for predicting cell-type disease genes and regulatory networks. *Genome Med* **13**, 95 (2021). https://doi.org/10.1186/s13073-021-00908-9

30 Dupacova, N., Antosova, B., Paces, J. & Kozmik, Z. Meis homeobox genes control progenitor competence in the retina. *Proceedings of the National Academy of Sciences of the United States of America* **118** (2021). https://doi.org/10.1073/pnas.2013136118

31 Negishi, Y. *et al.* Truncating mutation in NFIA causes brain malformation and urinary tract defects. *Hum Genome Var* **2**, 15007 (2015). https://doi.org/10.1038/hgv.2015.7

32 Silbereis, J. C., Pochareddy, S., Zhu, Y., Li, M. & Sestan, N. The Cellular and Molecular Landscapes of the Developing Human Central Nervous System. *Neuron* **89**, 248-268 (2016). https://doi.org/10.1016/j.neuron.2015.12.008

33 Cadwell, C. R. *et al.* Electrophysiological, transcriptomic and morphologic profiling of single neurons using Patch-seq. *Nat Biotechnol* **34**, 199-203 (2016). https://doi.org/10.1038/nbt.3445

34 Bos, J. L. Epac: a new cAMP target and new avenues in cAMP research. *Nat Rev Mol Cell Biol* **4**, 733-738 (2003). https://doi.org/10.1038/nrm1197

35 de Rooij, J. *et al.* Epac is a Rap1 guanine-nucleotide-exchange factor directly activated by cyclic AMP. *Nature* **396**, 474-477 (1998). https://doi.org/10.1038/24884

36 Woolfrey, K. M. *et al.* Epac2 induces synapse remodeling and depression and its disease-associated forms alter spines. *Nature neuroscience* **12**, 1275-1284 (2009). https://doi.org/10.1038/nn.2386

37 Zhu, Y. *et al.* Spatiotemporal transcriptomic divergence across human and macaque brain development. *Science* **362** (2018). https://doi.org/10.1126/science.aat8077

38 Consortium, G. T. Human genomics. The Genotype-Tissue Expression (GTEx) pilot analysis: multitissue gene regulation in humans. *Science* **348**, 648-660 (2015). https://doi.org/10.1126/science.1262110

39 Satterstrom, F. K. *et al.* Large-Scale Exome Sequencing Study Implicates Both Developmental and Functional Changes in the Neurobiology of Autism. *Cell* **180**, 568-584 e523 (2020). https://doi.org/10.1016/j.cell.2019.12.036

40 Katayama, Y. *et al.* CHD8 haploinsufficiency results in autistic-like phenotypes in mice. *Nature* **537**, 675-679 (2016). https://doi.org/10.1038/nature19357

41 Bernier, R. *et al.* Disruptive CHD8 mutations define a subtype of autism early in development. *Cell* **158**, 263-276 (2014). https://doi.org/10.1016/j.cell.2014.06.017

42 Durak, O. *et al.* Chd8 mediates cortical neurogenesis via transcriptional regulation of cell cycle and Wnt signaling. *Nature neuroscience* **19**, 1477-1488 (2016). https://doi.org/10.1038/nn.4400
43 Cotney, J. *et al.* The autism-associated chromatin modifier CHD8 regulates other autism risk genes during human neurodevelopment. *Nat Commun* **6**, 6404 (2015). https://doi.org/10.1038/ncomms7404
44 Sugathan, A. *et al.* CHD8 regulates neurodevelopmental pathways associated with autism spectrum disorder in neural progenitors. *Proceedings of the National Academy of Sciences of the United States of America* **111**, E4468-4477 (2014). https://doi.org/10.1073/pnas.1405266111
45 Gao, Y. *et al.* RGS6 Mediates Effects of Voluntary Running on Adult Hippocampal Neurogenesis. *Cell Rep* **32**, 107997 (2020). https://doi.org/10.1016/j.celrep.2020.107997
46 Kepecs, A. & Fishell, G. Interneuron cell types are fit to function. *Nature* **505**, 318-326 (2014). https://doi.org/10.1038/nature12983
47 Jones, K. A., Sumiya, M., Woolfrey, K. M., Srivastava, D. P. & Penzes, P. Loss of EPAC2 alters dendritic spine morphology and inhibitory synapse density. *Molecular and cellular neurosciences* **98**, 19-31 (2019). https://doi.org/10.1016/j.mcn.2019.05.001
48 Berry-Kravis, E., Hicar, M. & Ciurlionis, R. Reduced cyclic AMP production in fragile X syndrome: cytogenetic and molecular correlations. *Pediatr Res* **38**, 638-643 (1995). https://doi.org/10.1203/00006450-199511000-00002
49 Berry-Kravis, E. M. *et al.* Inhibition of phosphodiesterase-4D in adults with fragile X syndrome: a randomized, placebo-controlled, phase 2 clinical trial. *Nat Med* **27**, 862-870 (2021). https://doi.org/10.1038/s41591-021-01321-w
50 Wang, L. *et al.* A cross-species proteomic map reveals neoteny of human synapse development. *Nature* **622**, 112-119 (2023). https://doi.org/10.1038/s41586-023-06542-2

Acknowledgements

We thank Y. Xing, S. Krebsbach, D. Phan, M. Weidenfeller, and H. Thurston for technical assistance; K. Knobel at the Waisman IDD Model Core for core services; Dr. Heather Simmons, Director of Pathology Services (WNPRC) for non-human primate tissue acquisition; and the Birth Defects Research Laboratory (BDRL) at the University of Washington for human tissue acquisition. This work was supported by the National Institutes of Health **(**R01MH118827 and R01NS105200 to X.Z.; R01HD064743 to Q.C; R01NS064025, R01AG067025, and RF1MH128695 to D.W; 1R01HD106197 and UM1MH130991 to A.M.M.S; P51 OD011106 to WNPRC; P50HD105353 to Waisman Center; and R24HD000836 to BDRL). Further support was provided by the DOD IIRA grant (X.Z.), SFARI pilot grant (X.Z., A.M.M.S., Q.C., and D.W.),

Jenni and Kyle Professorship (X.Z.), Brain and Behavior Research Foundation (29721 to A.M.M.S.), Brain Research Foundation (BRFSG-2023-11 to A.M.M.S.), and the Medical Scientist Training Program T32 (GM140935 to R.D.R.).

Authors contributions

Y.G., Q.D., Q.C., X.Z., and A.M.M.S. conceived and designed the study. Y.G., Q.D., R.D.R., M.S., D.K.S., and A.M.M.S. performed the experiments. K.H.A., J.S., T.J., S.L., S.K., and D.W. analyzed the genomics data. J.E.L., D.D., I.G. provided the analyzed specimens. Y.G., Q.D., K.H.A., Q.C., X.Z., and A.M.M.S. wrote the manuscript. All authors edited the manuscript.

Competing Financial Interests

The authors declare that they have no competing interests.

Data and materials availability

The data genomic data has been submitted to GEO (GSE235493). The data can be interactively visualized at https://daifengwanglab.shinyapps.io/DevMacaquePFC/. All other data are available in the main paper or supplementary information.

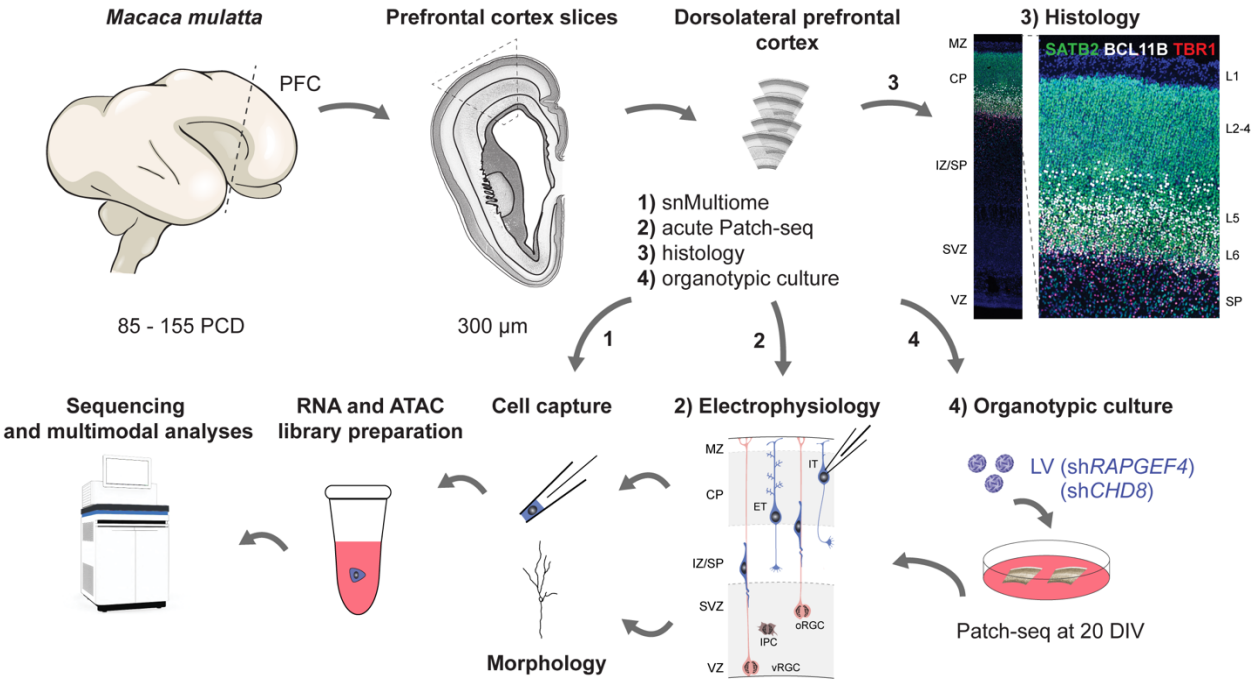

Fig. 1 | Schematic of the study design

The frontal cortex of Rhesus macaque (*Macaca mulatta*) brains, aged from postconceptional day (PCD) 85 to 155, were dissected and sectioned at 300 µm. Acute dorsolateral prefrontal cortices were analyzed using Patch-seq and single-nucleus multiome (snRNA-seq and snATAC-seq). Tissue from the same specimens, as well as human midfetal tissue, was also used to culture organotypic slices for functional analyses of select genes (*RAPGEF4* and *CHD8*). Validation of key findings was also performed by multiplexed immunostaining and single-molecule fluorescent in situ hybridization on dlPFC sections from the contralateral hemisphere of the same specimens (**Supplementary Table 1**). Finally, we have performed an integrative analysis of the generated multimodal dataset.

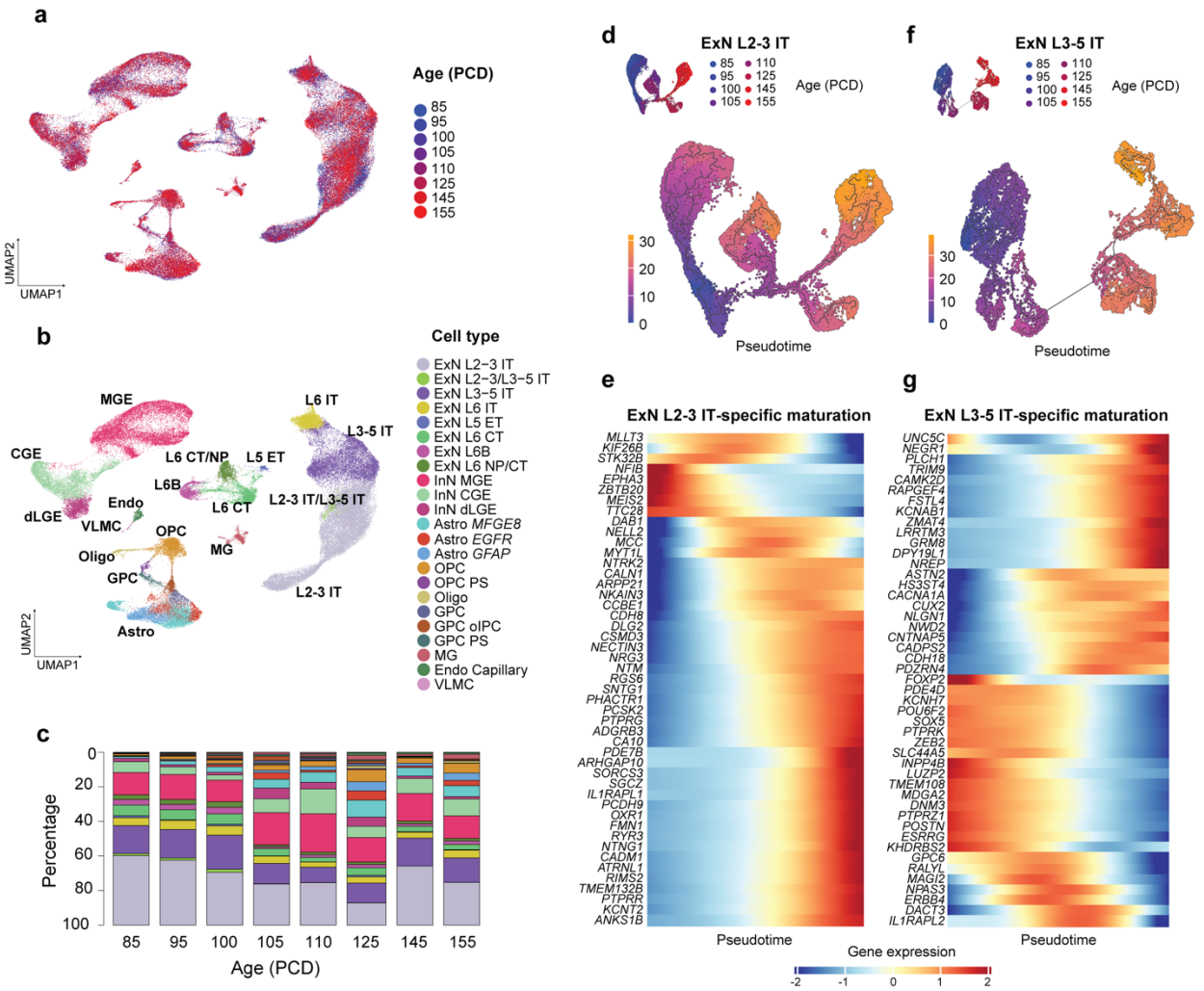

Fig. 2 | Single-nucleus transcriptomic atlas of rhesus macaque dlPFC cells across midfetal and late-fetal development. a-b, UMAP visualization of all the cell classes and subclasses. Cells are colored according to age in postconceptional days (PCD) (**a**) or cell subclass (**b**). **c**, Bar plot showing the cell composition of the dlPFC throughout midfetal and late-fetal development. **d**, UMAP visualization of the maturation trajectory of ExN L2-3 IT cells; the top panel is colored according to PCD, whereas the bottom panel is colored according to inferred pseudotime. **e**, Gene expression variation with pseudotime of genes specific to ExN L2-3 IT (from the top 100 highly variable genes along the developmental trajectory). **f**, UMAP visualization of the maturation trajectory of ExN L3-5 IT cells; top panel is colored according to PCD, whereas the bottom panel

is colored according to inferred pseudotime. **g**, Gene expression variation with pseudotime of genes specific to ExN L3-5 IT (from the top 100 highly variable genes along the developmental trajectory). ExN, excitatory neuronal cells; InN, inhibitory neuronal cells; IT, intratelencephalic; ET, extratelencephalic; CT, corticothalamic; NP, near-projecting; MGE, medial ganglionic eminence; CGE, caudal ganglionic eminence; dLGE, dorsal lateral ganglionic eminence; Astro, astrocytes; OPC, oligodendrocyte precursor cells; OPC PS, oligodendrocyte precursor cells in the proliferative stage; Oligo, oligodendrocytes; GPC, glial precursor cells; GPC oIPC, glial precursor – oligodendrocyte intermediate precursor cells; GPC PS, glial precursor cells in proliferative stage; MG, microglia; Endo, endothelial cells; VLMC, vascular leptomeningeal cells.

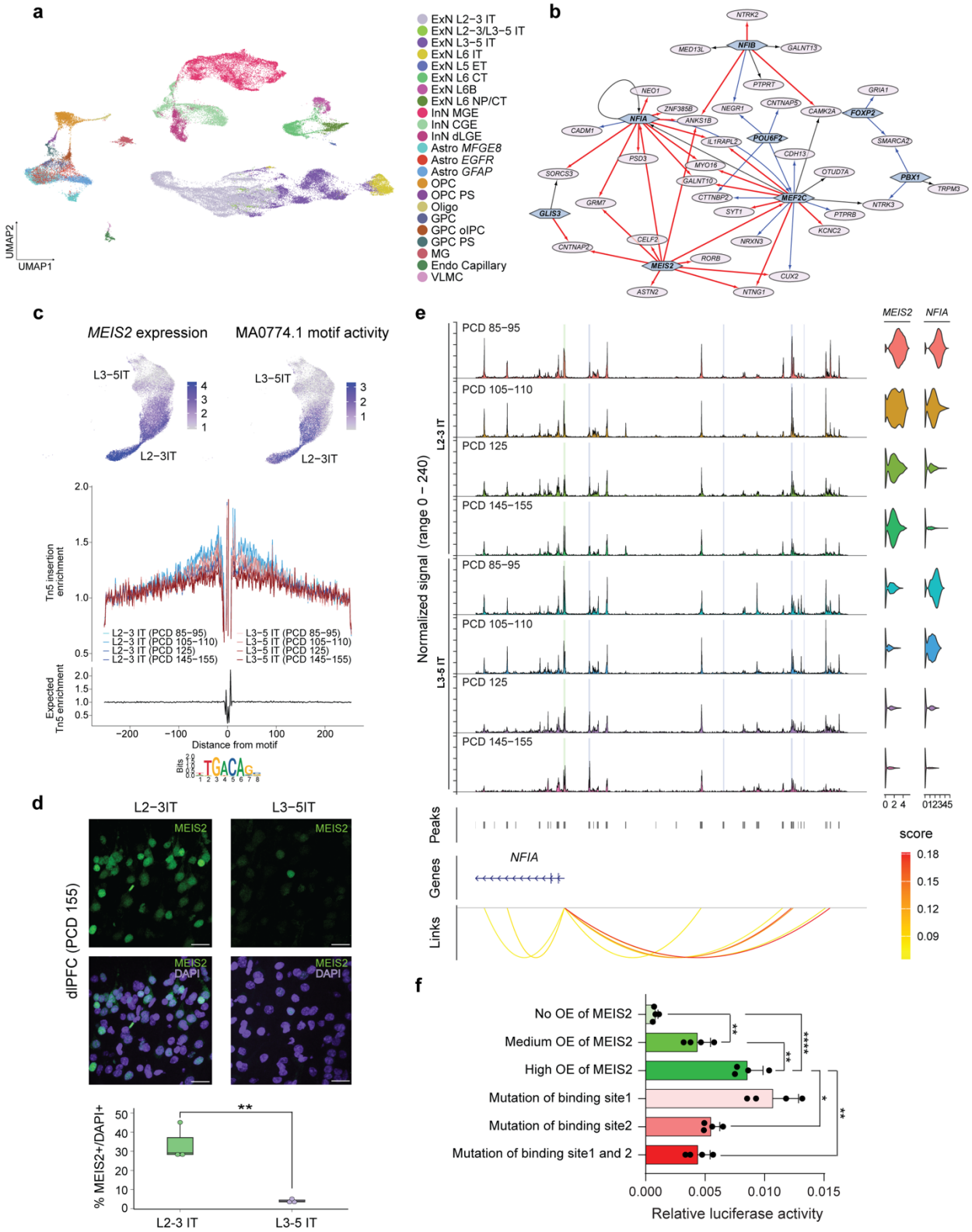
a
UMAP2
UMAP1
ExN L2−3 IT
ExN L2−3/L3−5 IT
ExN L3−5 IT
ExN L6 IT
ExN L5 ET
ExN L6 CT
ExN L6B
ExN L6 NP/CT
InN MGE
InN CGE
InN dLGE
Astro MFGE8
Astro EGFR
Astro GFAP
OPC
OPC PS
Oligo
GPC
GPC oIPC
GPC PS
MG
Endo Capillary
VLMC
b
NTRK2
NFIB
MED13L
GALNT13
PTPRT
NEO1
NFIA
ZNF385B
ANKS1B
NEGR1
CNTNAP5
CAMK2A
FOXP2
GRIA1
CADM1
IL1RAPL2
POU6F2
SMARCA2
PSD3
MYO16
CDH13
SORCS3
GALNT10
OTUD7A
PBX1
TRPM3
GLIS3
GRM7
CTTNBP2
MEF2C
NTRK3
SYT1
PTPRB
KCNC2
CELF2
NRXN3
CNTNAP2
RORB
MEIS2
CUX2
ASTN2
NTNG1
c
MEIS2 expression
MA0774.1 motif activity
L3−5IT
L2−3IT
Tn5 insertion enrichment
Expected Tn5 enrichment
L2−3 IT (PCD 85−95)
L2−3 IT (PCD 105−110)
L2−3 IT (PCD 125)
L2−3 IT (PCD 145−155)
L3−5 IT (PCD 85−95)
L3−5 IT (PCD 105−110)
L3−5 IT (PCD 125)
L3−5 IT (PCD 145−155)
Distance from motif
Bits
d
L2−3IT
L3−5IT
dlPFC (PCD 155)
MEIS2
DAPI
% MEIS2+/DAPI+
L2-3 IT
L3-5 IT
e
MEIS2
NFIA
PCD 85−95
PCD 105−110
PCD 125
PCD 145−155
L2-3 IT
L3-5 IT
Normalized signal (range 0 − 240)
Peaks
Genes
Links
score
f
No OE of MEIS2
Medium OE of MEIS2
High OE of MEIS2
Mutation of binding site1
Mutation of binding site2
Mutation of binding site1 and 2
Relative luciferase activity

Fig. 3 | Single-nucleus multiome gene expression and chromatin accessibility of rhesus macaque dlPFC cells across mid-late fetal development. a, Joint (snRNA-seq and snATAC-seq) UMAP visualization of cell subclasses. **b**, Differential gene regulatory networks inferred for ExN L2-3 IT and ExN L3-5 IT cell subclasses. Hexagonal nodes indicate transcription factors, and the elliptical nodes indicate the target genes. The edge colors represent the cell subclass specificity of transcription factor-target gene relationships (black, conserved in both cell subclasses, red, ExN L2-3 IT specific, blue – ExN L3-5 IT specific). **c**, UMAP visualization of *MEIS2* expression and motif activity scores for MA0774.1 (MEIS2 transcription factor motif) in L2-3 IT and L3-5 IT cells (top panels); MEIS2 transcription factor footprints for ExN L2-3 IT and ExN L3-5 IT cells across four developmental periods (bottom panel). **d**, Immunofluorescent detection of MEIS2 in the macaque dlPFC at PCD155, in L2-3 and L3-5 cells shows that a significantly higher number of cells express MEIS2 in L2-3 than in L3-5 (L3-5 was identified using in situ hybridization against *RORB*, as shown in **Extended Data Fig. 4e**). Scale bar, 20 µm. (**$p < 0.01$, *t*-test). **e**, Peak-to-gene link plot for *NFIA* together with the gene expression of *MEIS2* and *NFIA* in ExN L2-3 IT and ExN L3-5 IT across four developmental periods. The links indicate the co-activity links between *NFIA* gene expression and chromatin accessibility peaks. The highlighted regions within the chromatin accessibility peaks show the MEIS2 transcription factor motif (MA0774.1) binding sites. **f**, Dual-Luciferase reporter assay of *NFIA* genomic sequences containing MEIS2 motifs. OE, overexpression. *$p < 0.05$, **$p < 0.01$, ****$p < 0.0001$ (one-way analysis of variance with Tukey multiple comparisons). Each dot represents one replicate.

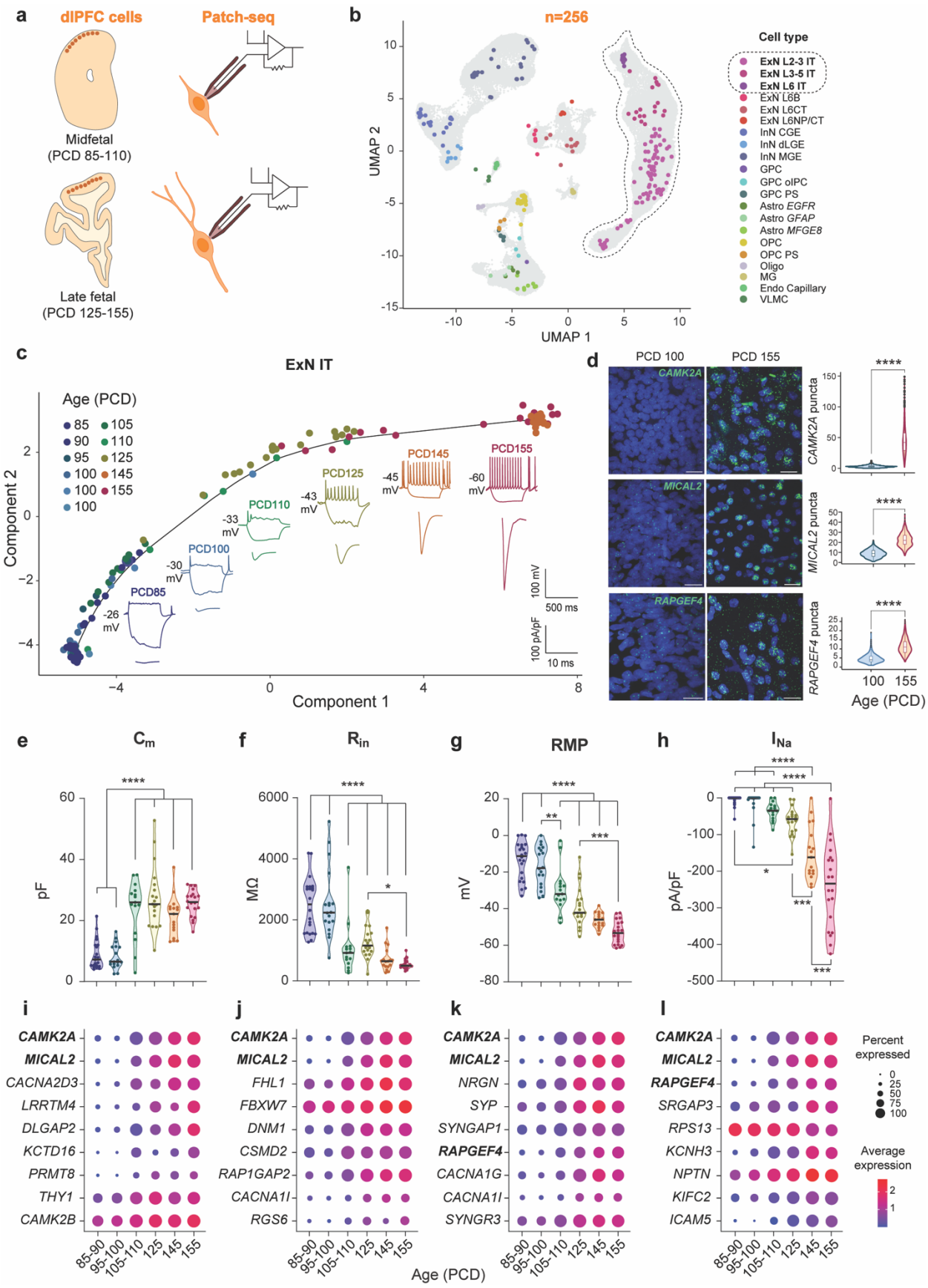
a
dlPFC cells
Patch-seq
Midfetal
(PCD 85-110)
Late fetal
(PCD 125-155)
b
n=256
UMAP 2
UMAP 1
Cell type
ExN L2-3 IT
ExN L3-5 IT
ExN L6 IT
ExN L6B
ExN L6CT
ExN L6NP/CT
InN CGE
InN dLGE
InN MGE
GPC
GPC oIPC
GPC PS
Astro EGFR
Astro GFAP
Astro MFGE8
OPC
OPC PS
Oligo
MG
Endo Capillary
VLMC
c
ExN IT
Age (PCD)
85
90
95
100
100
100
105
110
125
145
155
Component 2
Component 1
PCD85
PCD100
PCD110
PCD125
PCD145
PCD155
-26 mV
-30 mV
-33 mV
-43 mV
-45 mV
-60 mV
100 mV
500 ms
100 pA/pF
10 ms
d
PCD 100
PCD 155
CAMK2A
MICAL2
RAPGEF4
CAMK2A puncta
MICAL2 puncta
RAPGEF4 puncta
Age (PCD)
e
Cm
pF
f
Rin
MΩ
g
RMP
mV
h
INa
pA/pF
i
j
k
l
CAMK2A
MICAL2
CACNA2D3
LRRTM4
DLGAP2
KCTD16
PRMT8
THY1
CAMK2B
FHL1
FBXW7
DNM1
CSMD2
RAP1GAP2
CACNA1I
RGS6
NRGN
SYP
SYNGAP1
RAPGEF4
CACNA1G
CACNA1I
SYNGR3
SRGAP3
RPS13
KCNH3
NPTN
KIFC2
ICAM5
85-90
95-100
105-110
125
145
155
Age (PCD)
Percent expressed
Average expression

Fig. 4 | Identification of midfetal and late-fetal neuronal maturation-related genes using Patch-seq. a, Schematic representation of the Patch-seq experimental design for analyzing midfetal and late-fetal rhesus macaque dlPFC cells. **b,** Integration of the 256 cells profiled by Patch-seq onto the snRNA-seq reference UMAP. **c,** Pseudotime trajectory based on the gene expression profiles of patched IT neurons from 16 individual rhesus macaque fetal brains at 11 distinct fetal ages, with representative electrophysiological sample traces (voltage responses to depolarizing and hyperpolarizing current injections, and inward sodium currents). **d,** In situ hybridization detection and quantification (right panel) of *CAMK2A*, *MICAL2*, and *RAPGEF4* in PCD100 and PCD155 dlPFC. Scale bar, 20 µm. (****$p < 0.0001$, *t*-test). **e-l,** Plots illustrating the developmental changes in electrophysiological properties, including membrane capacitance (C_m, **e**), input resistance (R_{in}, **f**), resting membrane potential (RMP, **g**), and inward sodium current (I_{Na}, **h**) of IT neurons across six different age groups. Bottom panels show the expression levels of C_m-correlated genes (**i**), R_{in}-correlated genes (**j**), RMP-correlated genes (**k**), and I_{Na}-correlated genes (**l**) in IT neurons across the same age groups. (**$p < 0.01$, ***$p < 0.001$, ****$p < 0.0001$, one-way ANOVA, Tukey's multiple comparisons test).

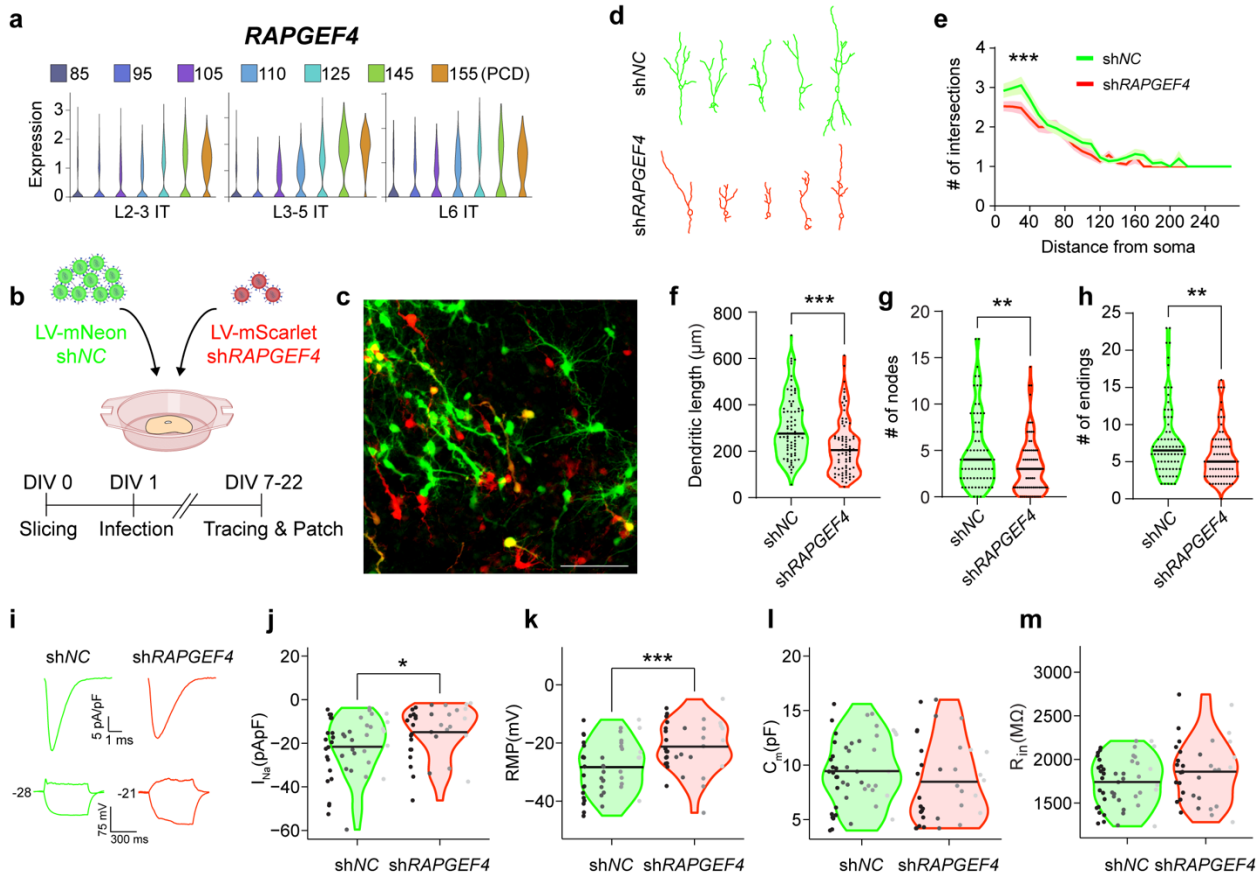

Fig. 5 | Knockdown of *RAPGEF4* impairs morphological and electrophysiological maturation of cortical neurons in macaque organotypic dlPFC slices. a, Violin plots showing the expression of *RAPGEF4* in IT neurons from PCD85 to PCD155. **b,** Schematic of the experimental setup for investigating the morphological and electrophysiological alterations after *RAPGEF4* knockdown in ex vivo dlPFC slices. **c,** Representative image depicting *RAPGEF4* knockdown (mScarlet^{+}[red], mScarlet^{+}/mNeon^{+}[yellow]) and control (mNeon^{+}[green only]) neurons in macaque dlPFC slices. Scale bar, 100 μm. **d,** Sample traces depicting the morphology of both *RAPGEF4* knockdown (bottom panel) and control (top panel) neurons. **e,** Sholl analysis of dendritic complexity in *RAPGEF4* knockdown neurons compared to control neurons [$F(1,150) = 14.531$, ***$p < 0.001$, multivariate analysis of variance]. **f-h**, Knockdown of *RAPGEF4* decreases total dendritic length(**f**), number of nodes(**g**), and number of endings(**h**) (*t*-test, ***p <

0.001, **p < 0.01). **i**, Representative traces of inward sodium currents and voltage responses to depolarizing and hyperpolarizing current injections for *RAPGEF4* knockdown (right panel) and control (left panel) neurons. **j-m,** Knockdown of *RAPGEF4* leads to increased I_{Na} (**j**) and RMP (**k**), without significantly change in C_m (**l**) and R_{in} (**m**) (*t*-test, ***p < 0.001, *p < 0.05). Each dot represents one patched cell. All cells were collected from four individual fetal brains, with each fetal brain indicated by a different color: black, dark gray, medium gray, and light gray.

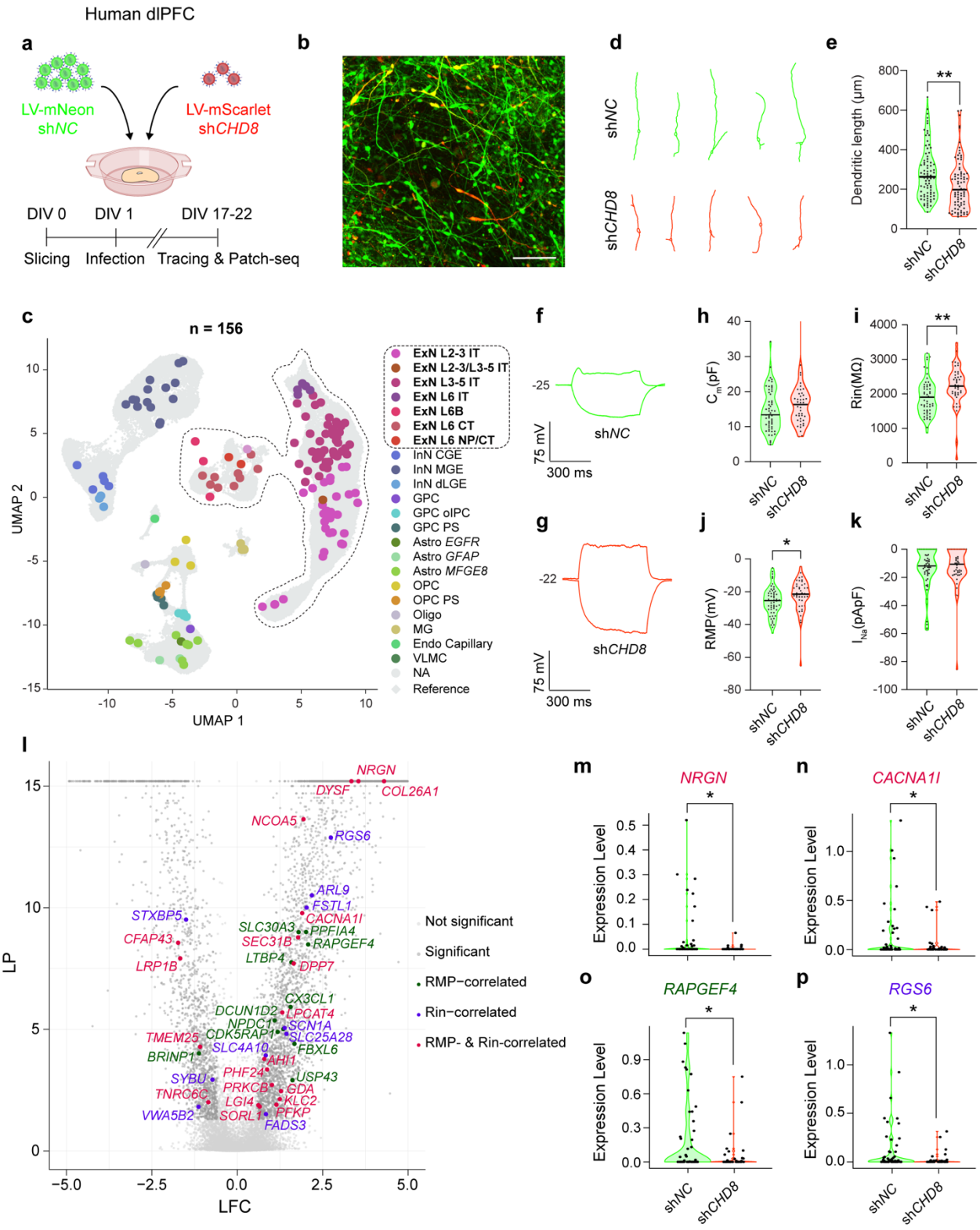
Human dlPFC
a
LV-mNeon
shNC
LV-mScarlet
shCHD8
DIV 0
DIV 1
DIV 17-22
Slicing
Infection
Tracing & Patch-seq
b
d
shNC
shCHD8
e
Dendritic length (μm)
**
shNC
shCHD8
c
n = 156
UMAP 2
UMAP 1
ExN L2-3 IT
ExN L2-3/L3-5 IT
ExN L3-5 IT
ExN L6 IT
ExN L6B
ExN L6 CT
ExN L6 NP/CT
InN CGE
InN MGE
InN dLGE
GPC
GPC oIPC
GPC PS
Astro EGFR
Astro GFAP
Astro MFGE8
OPC
OPC PS
Oligo
MG
Endo Capillary
VLMC
NA
Reference
f
-25
75 mV
300 ms
shNC
g
-22
75 mV
300 ms
shCHD8
h
Cm(pF)
shNC
shCHD8
i
Rin(MΩ)
**
shNC
shCHD8
j
RMP(mV)
*
shNC
shCHD8
k
INa(pApF)
shNC
shCHD8
l
LP
LFC
NRGN
DYSF
COL26A1
NCOA5
RGS6
ARL9
FSTL1
CACNA1I
STXBP5
SLC30A3
PPFIA4
CFAP43
SEC31B
RAPGEF4
LTBP4
DPP7
LRP1B
CX3CL1
DCUN1D2
LPCAT4
NPDC1
SCN1A
TMEM25
CDK5RAP1
SLC25A28
SLC4A10
FBXL6
BRINP1
AHI1
SYBU
PHF24
USP43
TNRC6C
PRKCB
GDA
LGI4
KLC2
VWA5B2
SORL1
PFKP
FADS3
Not significant
Significant
RMP−correlated
Rin−correlated
RMP- & Rin-correlated
m
NRGN
Expression Level
*
n
CACNA1I
Expression Level
*
o
RAPGEF4
Expression Level
*
p
RGS6
Expression Level
*
shNC
shCHD8

Fig. 6 | Knockdown of *CHD8* impairs maturation of cortical excitatory neurons and down-regulates *RAPGEF4* in human organotypic dlPFC slices. a, Schematic diagram illustrating the experimental setup used to study the morphological and electrophysiological changes after knockdown of *CHD8* in ex vivo human fetal cortical slices. **b**, Representative image showing *CHD8* knockdown (mScarlet+[red], mScarlet+ and mNeon+[yellow]) and control ($mNeon^{+}$[green]) neurons in human cortical slices. Scale bar, 100 μm. **c**, Integration of the 156 cells profiled by Patch-seq onto the snRNA-seq reference UMAP. **d**, Sample traces showing the morphology of both *CHD8* knockdown and control neurons. **e**, *CHD8* knockdown reduces total dendritic length (**$p < 0.01$, *t*-test). **f**, **g**, Representative traces (voltage response to depolarizing [50 pA] and hyperpolarizing [-50 pA] current injections) for control neurons (**f**) and *CHD8* knockdown (**g**). **h**-**k**, *CHD8* knockdown increases R_{in} (**i**) and RMP (**j**) but does not significantly alter C_m (**h**) and I_{Na} (**k**) (*$p < 0.05$, **$p < 0.01$, *t*-test). **l**, Volcano plot depiction ($-\log_{10}(P_{adj})$ vs $\log_2$(*fold-change*)) of differentially expressed genes between LV-sh*NC* and LV-sh*CHD8* -infected excitatory neurons. Genes with expression profiles that significantly correlate with the RMP (green), R_{in} (purple), or both (red) electrophysiology features are labeled. **m-p,** Violin plots showing the expression levels of *NRGN* (**m**), *CACNA1I* (**n**), *RAPGEF4* (**o**), and *RGS6* (**p**), highlighting the effect of *CHD8* knockdown on these neuronal maturation genes (**Fig. 4i-l**).